GSA Supplemental Information

Mass balance controls on sediment scour and bedrock erosion in waterfall plunge pools

J.S. Scheingross[1*] and M.P. Lamb[2]

[1]Deperatment of Geological Sciences and Engineering, University of Nevada Reno

[2]Division of Geological and Planetary Sciences, California Institute of Technology

*jscheingross@unr.edu

SUPPLEMENTAL INFORMATION

Flow hydraulics in channel reaches adjacent to waterfalls

We assume identical geometry of the reaches above and below the waterfall, as is common in narrow bedrock canyons, and steady, uniform flow such that

$$\tau_{river} = \rho g H S = \rho C_{f\_river} U^2 \quad \text{(S1)}$$

and

$$\tau_* = HS/RD \quad \text{(S2)}$$

Here, τ_{river} is the river shear stress, ρ is water density, g is gravitational acceleration, H is reach-averaged flow depth, S is the river slope, U is depth-averaged water velocity, R is the submerged sediment density (R=1.65 for quartz), D is the median grain size, and τ_* is the Shields stress. C_{f_river} is the river friction factor, which we solve for as (Garcia, 2008)

$$C_{f\_river} \equiv \left(\frac{u_*}{U}\right)^{1/2} = \left[8.1\left(\frac{H}{3D}\right)^{1/6}\right]^{-2} \quad \text{(S3)}$$

where $u_* = (\tau_{river}/\rho)^{1/2}$ is the shear velocity. We solve for H by combining equations (S1) and (S3) and assuming conservation of mass ($Q_w = UWH$, where W is channel width). This approach ignores friction from the walls, which may be substantial for deep, narrow flows in bedrock canyons (e.g., Nelson and Seminara, 2011).

Waterfall plunge pool sediment transport capacity

We calculate the sediment transport capacity of waterfall plunge pools following Scheingross and Lamb (2016) which assumes steady, axisymmetric flow within a cylindrical plunge with vertical bedrock walls. The presence of vertical walls requires sediment to be suspended up and over the pools in order to be transported out of the pool. The model combines jet hydraulic theory and sediment suspension theory to predict the plunge pool sediment concentration under transport-limited conditions as

$$c(r,z) = c_b \exp\left(-\frac{(z - z_{mixed})}{L_d}\right)\left(\frac{I_0(r/L_d) + \frac{I_1(r/L_d)}{K_1(r/L_d)}K_o(r/L_d)}{I_0(\delta/L_d) + \frac{I_1(r/L_d)}{K_1(r/L_d)}K_0(\delta/L_d)}\right) \quad \text{(S4)}$$

where r and z are radial and vertical coordinates, respectively, c_b is the near bed sediment concentration that is solved for using standard sediment entrainment theory (Eq. 30 in Scheingross and Lamb (2016)), z_{mixed} is the height of the well-mixed layer of sediment near the pool floor and is assumed to be set by the height of sediment saltation following Sklar and Dietrich (2004), L_d parameterizes sediment mixing through a diffusive length scale which balances turbulence and particle settling, and δ is the radius of the region within the plunge pool in which flow is primarily downward due to advection from the descending jet. The notation I_0, K_0, I_1, and K_1 in Eq. (S4) denote modified Bessel functions of the first and second kind of order 0 and 1, respectively.

Plunge pool sediment transport capacity (Q_{sc_pool}) is predicted as

$$Q_{sc\_pool} = \frac{Q_w}{(z_{water} - z_{lip})} \int_{z=z_{lip}}^{z=z_{water}} c(r_{pool}, z)dz \quad \text{(S5)}$$

where z_{water} and z_{lip} are the elevation of the water surface and the plunge pool lip, respectively, and r_{pool} is the plunge pool radius. The Scheingross and Lamb (2016) theory shows that plunge pool sediment transport capacity can be predicted from four non-dimensional variables

$$\frac{Q_{sc\_pool}}{Q_w} = f\left(\frac{\tau_{*pool}}{\tau_{*c\_pool}}, \frac{(z_{lip} - z_{mixed})}{L_d}, \frac{r_{pool}}{L_d}, \frac{\delta}{L_d}\right) \qquad \text{(S6)}$$

Where τ_{*pool} and τ_{*c_pool} are the Shields stress and critical Shields stress within the plunge pool, respectively. Scheingross and Lamb (2016) tested the theory against flume experiments and found good agreement across the range of these non-dimensional variables that are commonly observed in the field (see Figure 4 in Scheingross and Lamb (2016)).

The model of Scheingross and Lamb (2016) assumes that the waterfall jet falls a finite distance in freefall (i.e., the bedrock step composing the waterfall is emerged from the flow) and that the full waterfall jet enters the plunge pool. At very large discharges, these assumptions can be violated as the flow depth below the waterfall can exceed the waterfall drop height and the jet diameter can grow larger than that of the plunge pool. Under these cases, we refrain from predicting waterfall plunge pool sediment transport capacity.

River sediment transport capacity

We calculated river sediment transport capacity following Lamb et al (2008). This method calculates the total river sediment transport capacity, Q_{sc_river}, as the sum of the bedload and suspended load transport capacities, where suspended load transport capacity is calculated by integrating the product of the sediment concentration and velocity profiles. Following this method, river sediment transport capacity can be solved for by re-arranging Equation 20 from Lamb et al (2008)

$$Q_{sc\_river} = \frac{Q_{sc\_BL}(UH\chi + U_b H_b)}{U_b H_b} \text{ (S7)}$$

where Q_{sc_BL} is bedload transport capacity, U_b and H_b are the bedload velocity and height of the bedload layer, respectively, and χ is the integral that describes the vertical structure of the flow velocity and sediment concentration. We calculate the bedload transport capacity following Fernandez Luque and van Beek (1976)

$$Q_{sc\_BL} = 5.7(W)(RgD^3)^{0.5}(\tau_* - \tau_{*c})^{1.5} \text{ (S8)}$$

where τ_{*c} is the critical Shields stress for motion, and follow Lamb et al (2008) to calculate U, H, U_b,, H_b, and χ. Finally, we assumed channel width at a site is constant with varying discharge, as waterfalls often occur in steep-walled canyons.

Influence of grain size mixtures

Size-selective transport has yet to be examined in bedrock plunge pools; however, we expect that partial transport of fines during low flows in rivers (Hassan and Church, 2001; Scheingross et al., 2013) can explain the observations of plunge pools filled with fine sediment (Fig. 1 and S1). When the waterfall jet is weak, shear stress on the pool floor can be negligible, making pools traps of even the finest sediment. In contrast, mountain streams often transport a wide distribution of grain sizes during large floods (e.g., Rickenmann et al., 2012). Thus, size-selective transport may explain the observation of coarse bars at pool boundaries (Fig. 1 and S1), because bars form at high discharge capable of transporting coarse sediment, and size-selective disentrainment of sediment favors coarse grain deposition (Fedele and Paola, 2007). Fine sediment may also be winnowed from the bar during low flow when sediment transport is active in the river, but not the pool, which is further consistent with the existence of coarse sediment bars at the downstream pool boundary. For these reasons, we expect size-selective transport in the presence of sediment mixtures should yield similar results to our single grain size modeling.

The presence of sediment mixtures may also change the dynamics of sediment transport (e.g., Parker, 2008), as has been observed in alluvial scour pools where wider grain size distributions create deeper pools (Pagliara et al., 2006). Further investigation of how sediment mixtures influence the fill and scour of bedrock-walled plunge pools remains a key target for future work. However, if the observations of Pagliara et al. (2006) hold, they imply the presence of sediment mixtures would increase the discrepancy between plunge pool and river sediment transport capacity due to the increase in plunge pool depth, thereby accentuating the results presented here.

***Solving for* $\mathbf{Q_{w\_scour}}$**

We solve for the critical discharge necessary to scour sediment from plunge pools, Q_{w_scour}, numerically by finding the discharge for which Q_{sc_river}=Q_{sc_pool} using estimates of the plunge pool geometry. We use particle size and the geometrics of the channel, waterfall and plunge pool to solve for Q_{sc_river} following Eq. (S7) and Q_{sc_pool} following Scheingross and Lamb (2016) for 500 logarithmically spaced water discharges between 10^{-1} and 10^{4} m^3/s. We then identify the water discharge for which Q_{sc_river}=Q_{sc_pool} by finding the point of intersection between the Q_{sc_river}-discharge and Q_{sc_pool}-discharge curves. When using plunge pool bedrock geometry (i.e., the depth to the bedrock pool floor and the radius from the pool center to its bedrock sidewall), Q_{w_scour} represents the threshold discharge needed to scour all sediment from the pool, expose the bedrock bed, and allow for vertical bedrock incision via sediment impacts.

In some cases, the discharge needed for pools to scour to bedrock was so great that waterfalls became submerged and/or waterfall jets became wider than the plunge pools they fed into. These conditions violate the assumptions of the Scheingross and Lamb (2016), and we are unable to predict Q_{w_scour}. For these cases, we instead place a minimum bound on Q_{w_scour} using the maximum discharge at which the assumptions of the Q_{sc_pool} model has not been violated, and for which $Q_{sc\_pool} < Q_{sc\_river}$ (Fig. S4). Figure 4 in the main text lumps both cases where Q_{w_scour} is directly calculated, and cases where a minimum estimate of Q_{w_scour} is made, thereby providing a conservative estimate of the return period necessary for waterfalls to scour to bedrock (that is, the lumping of these two metrics biases the results towards lower return periods). We explicitly separate these two cases in Figure S3 and Table S1.

Our calculation of the threshold discharge to allow bedrock erosion in plunge pools uses the field-surveyed waterfall height, plunge pool bedrock radius, channel geometry, and grain size reported in Scheingross and Lamb (2016). These pools typically had well-exposed bedrock walls allowing accurate measurements of plunge pool bedrock radii, but were often filled or partially-filled with sediment at the time of our surveying (including at the Middle Switzer Falls reference site), such that the true depth to bedrock is only known for 5 of the 75 waterfalls. For the remaining 70 waterfalls, we set pool depth equal to the pool bedrock radius for cases in which existing depth measurements were less than the radius. Experiments of plunge pool bedrock erosion suggest that waterfalls typically erode deep, narrow pools, with depths that can be greater than three times the plunge pool radius (Scheingross et al., 2017). Setting pool depth equal to pool radius is thus a purposely conservative estimate of the true depth, as this biases estimates of Q_{w_scour} for bedrock erosion towards lower discharges, and thus strengthens our argument that plunge pool bedrock erosion typically requires infrequent, large magnitude events (Fig. 4). Using the reported plunge pool depths in the Scheingross and Lamb (2016) database instead of the pool radii would still result in 44 of the 75 pools requiring floods with recurrence intervals greater than 10 y to scour below the maximum reported depth for conditions of $Q_{s\_river}/Q_{sc\_river} = 1$.

We determined the recurrence interval of flows large enough to erode bedrock in pools (or, in cases where the Scheingross and Lamb (2016) model assumptions were violated, the minimum bound on Q_{w_scour} for bedrock erosion) by linearly interpolating along the discharge-frequency relations we created at each waterfall using historical water discharge records. We assumed a linear scaling between discharge and drainage area to account for the fact that gages and waterfalls were not co-located. When available, we used discharge records covering greater than 20 y from instrument gages on the same river as the waterfall of interest; where such records did not exist, we used records from nearby gages (Table S1). For cases where, the threshold discharge to erode bedrock exceeded the maximum discharge on record, and we set the recurrence interval equal to one year greater than the length of the discharge record (Table S1)

In some cases, the plunge pool sediment transport capacity was greater than the river sediment transport capacity across all discharges, there was no crossing of the plunge pool and river sediment transport capacity curves, and therefore no estimate of the threshold discharge for bedrock erosion. This behavior suggests disequilibrium plunge pool bedrock geometries, which may be a consequence of our conservatively low estimates for pool depth or indicate the presence of newly formed pools, and occurred for 6, 8, and 17 pools when setting Q_{s_river} / Q_{sc_river} equal to 1, 0.5, and 0.1, respectively. For an additional 17 plunge pools with Q_{s_river} / Q_{sc_river} equal to 1 (and 0 cases when Q_{s_river} / Q_{sc_river} was 0.5 or 0.1), curves crossed at two locations coinciding with Q_{w_agg} and Q_{w_scour} (e.g., Fig. 2C). For these cases, we calculated the threshold discharge for bedrock erosion at the higher crossing value (i.e, Q_{w_scour}). The lower crossing point (i.e., Q_{w_agg}) is typically coincident with the threshold discharge for sediment transport in adjacent river reaches (Fig. 2C); thus, even though pools have capacity to scour sediment at these low discharges, they lack upstream sediment supply, and hence have no or negligible availability of tools for bedrock erosion. In contrast, at discharges above Q_{w_scour}, there is both sediment supply and exposure of bedrock, allowing for efficient bedrock erosion.

SUPPLEMENTAL TABLES

We provide the Supplemental Tables at the end of this PDF to facilitate ease of reference and preservation. Supplemental tables are also provided in a separate file in .xlsx format for ease of access.

Table S1: Field-surveyed waterfall plunge pools from Scheingross and Lamb (2016).

Table S2: Individual clast measurements for grain size distributions shown in Figure 1.

REFERENCES CITED:

Chatanantavet, P., Whipple, K. X., Adams, M. A., and Lamb, M. P., 2013, Experimental study on coarse grain saltation dynamics in bedrock channels: Journal of Geophysical Research-Earth Surface, v. 118, no. 2, p. 1161-1176.

Fedele, J. J., and Paola, C., 2007, Similarity solutions for fluvial sediment fining by selective deposition: Journal of Geophysical Research-Earth Surface, v. 112, no. F2.

Ferguson, R. I., and Church, M., 2004, A simple universal equation for grain settling velocity: Journal of Sedimentary Research, v. 74, no. 6, p. 933-937.

Fernandez Luque, R., and van Beek, R., 1976, Erosion and transport of bed-load sediment: Journal of Hydraulic Research, v. 14, p. 127-144.

Garcia, M. H., 2008, Sediment transport and morphodynamics, *in* Garcia, M. H., ed., Sedimentation Engineering: Processes, Measurements, Modeling, and Practice: Reston, Virginia, American Society of Civil Engineers.

Graf, W. H., and Cellino, M., 2002, Suspension flows in open channels; experimental study: Journal of Hydraulic Research, v. 40, no. 4, p. 435-447.

Hassan, M. A., and Church, M., 2001, Sensitivity of bed load transport in Harris Creek: Seasonal and spatial variation over a cobble-gravel bar: Water Resources Research, v. 37, no. 3, p. 813-825.

Lamb, M. P., Dietrich, W. E., and Sklar, L. S., 2008, A model for fluvial bedrock incision by impacting suspended and bed load sediment: Journal of Geophysical Research-Earth Surface, v. 113, no. F3.

Nelson, P. A., and Seminara, G., 2011, Modeling the evolution of bedrock channel shape with erosion from saltating bed load: Geophysical Research Letters, v. 38.

Pagliara, S., Hager, W. H., and Minor, H. E., 2006, Hydraulics of plane plunge pool scour: Journal of Hydraulic Engineering-Asce, v. 132, no. 5, p. 450-461.

Parker, G., 2008, Transport of gravel and sediment mixtures, *in* Garcia, M. H., ed., Sedimentation Engineering: Processes, Measurements, Modeling, and Practice: Reston, Virginia, American Society of Civil Engineers.

Rickenmann, D., Turowski, J. M., Fritschi, B., Klaiber, A., and Ludwig, A., 2012, Bedload transport measurements at the Erlenbach stream with geophones and automated basket samplers: Earth Surface Processes and Landforms, v. 37, no. 9, p. 1000-1011.

Scheingross, J. S., Brun, F., Lo, D. Y., Omerdin, K., and Lamb, M. P., 2014, Experimental evidence for fluvial bedrock incision by suspended and bedload sediment: Geology, v. 42, no. 6, p. 523-526.

Scheingross, J. S., and Lamb, M. P., 2016, Sediment transport through self-adjusting, bedrock-walled waterfall plunge pools: J. Geophys. Res. Earth Surf., v. 121.

Scheingross, J. S., Lo, D. Y., and Lamb, M. P., 2017, Self-formed waterfall plunge pools in homogeneous rock: Geophysical Research Letters, v. 44, no. 1, p. 200-208.

Scheingross, J. S., Winchell, E. W., Lamb, M. P., and Dietrich, W. E., 2013, Influence of bed patchiness, slope, grain hiding, and form drag on gravel mobilization in very steep streams: Journal of Geophysical Research-Earth Surface, v. 118, no. 2, p. 982-1001.

Sklar, L. S., and Dietrich, W. E., 2004, A mechanistic model for river incision into bedrock by saltating bed load: Water Resources Research, v. 40, no. 6.

Figure S1: Waterfall plunge-pool systems with fine sediment fills and coarse sediment bars from the San Gabriel Mountains, CA with grain size distributions shown in Figure 1. Plunge pool 1 (A) and 2 (B) on Arroyo Seco. Large grains in foreground of (A) have a median diameter of ~20 cm for scale. (C) Wolfskill Falls, San Dimas Experimental Forest.

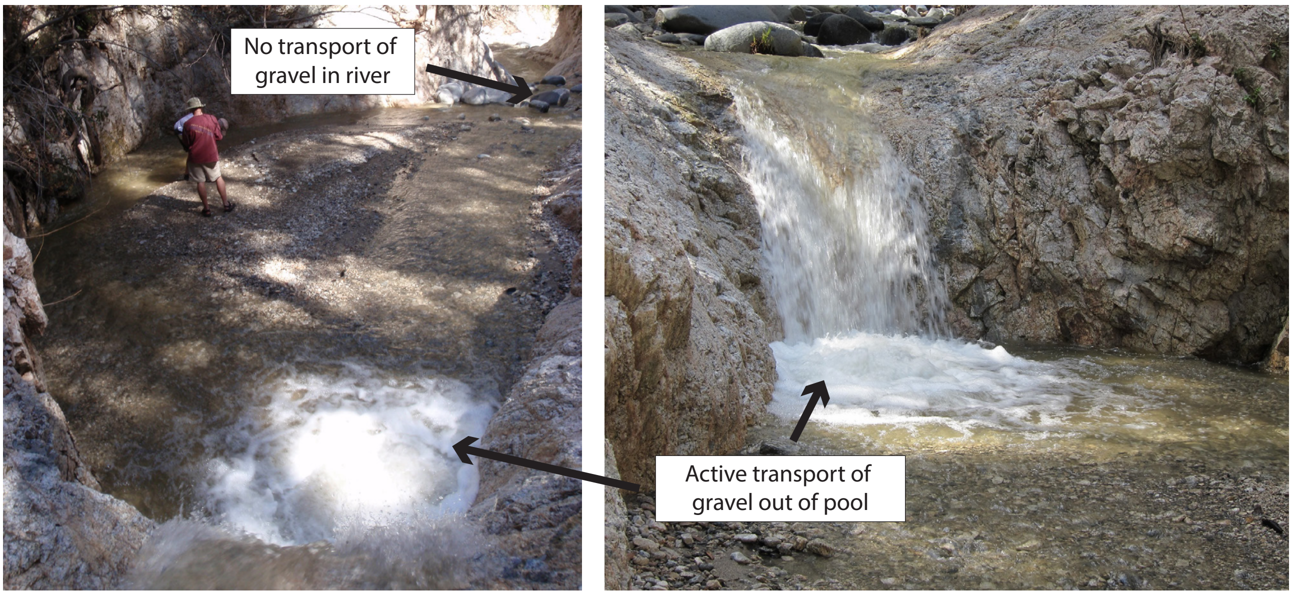

Figure S2: Example of waterfall plunge pool on Arroyo Seco, California. Photos taken in March 2010 and show the plunge pool filled with fine sediment following the Station Fire (August 2009). Field observations showed active transport of gravel out of the pool, but no gravel transport in the downstream river, consistent with our model predictions for shallow pools (Fig. 2C).

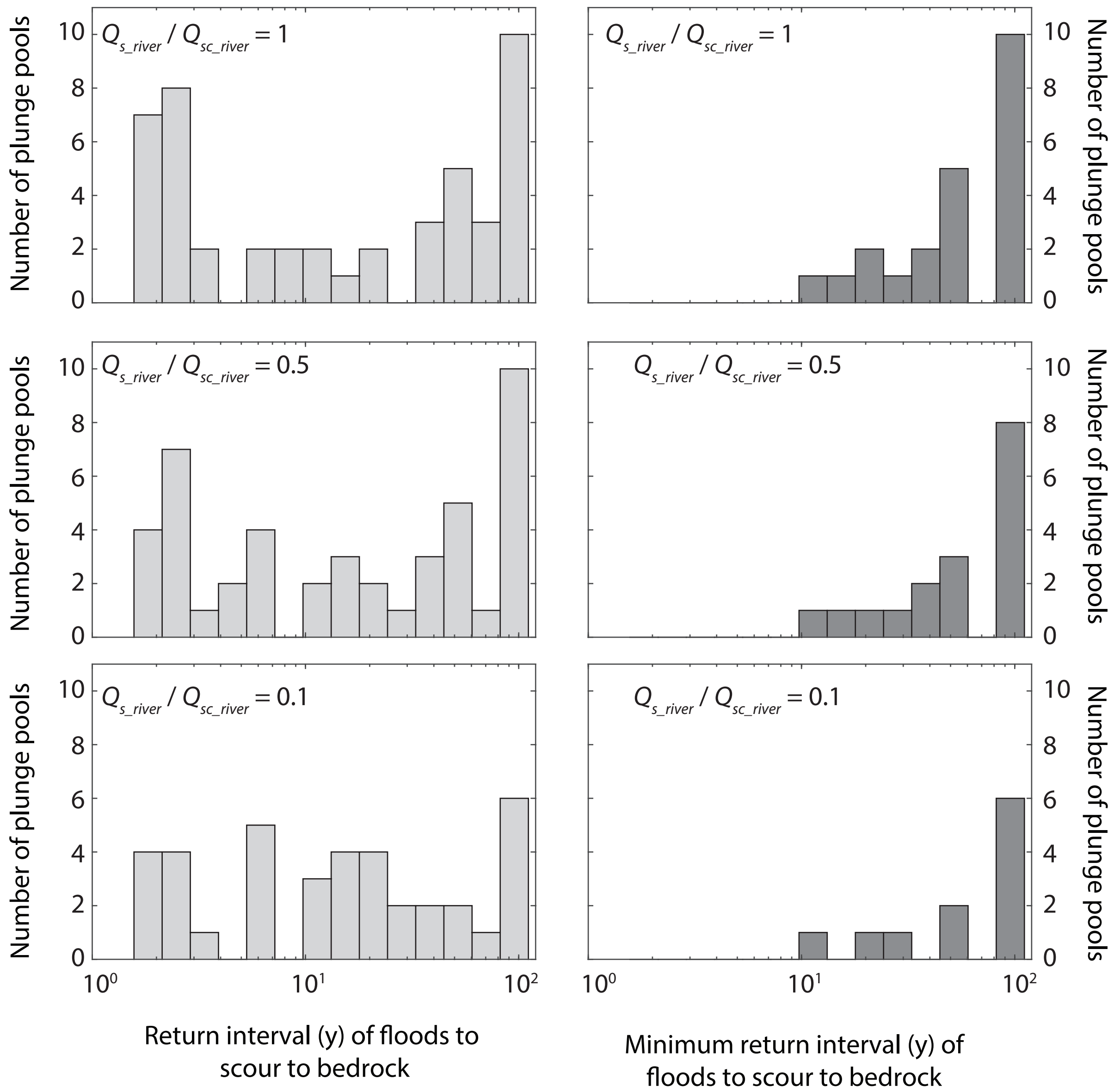

Figure S3: (Left column) Histogram of flood return interval for plunge pools in which the critical discharge to scour all sediment from pools and erode bedrock can be estimated. (Right column) Histogram of flood return interval for plunge pools where the waterfall becomes submerged prior to the onset of bedrock erosion. For these cases, we use the discharge of waterfall submergence as a minimum estimate of the threshold discharge to scour to bedrock. All calcluations use τ_{*c_pool} = 0.045, and we varied Q_{s_river} / Q_{sc_river} from 0.1 to 1 as indicated in each panel. Historgrams omit cases in which is Q_{sc_pool} greater than Q_{sc_river} at all discharges, as these likely reflect disequilibrium plunge-pool geometries.

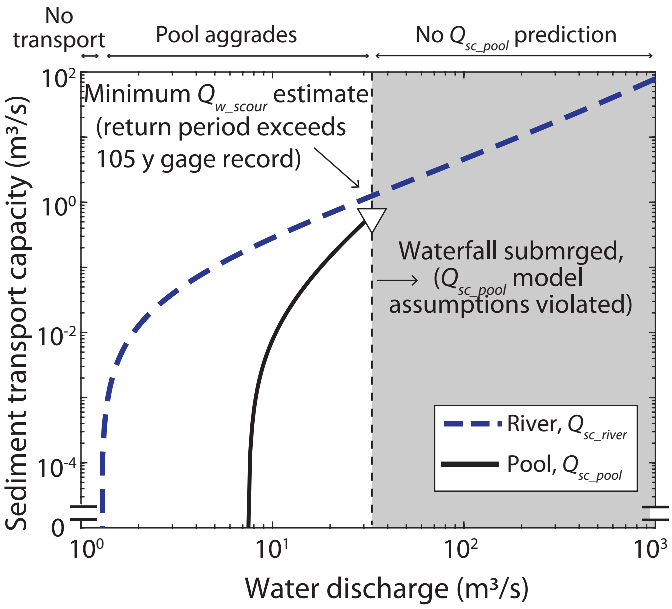

Figure S4: Example comparisons of river and plunge-pool sediment-transport capacities for a case where the waterfall becomes submerged before the pool is predicted to scour to bedrock, violating assumptions of the Scheingross and Lamb (2016) model (Waterfall DC2, Table S1). In this case, the discharge required to submerged the waterfall is ~4 times larger than the maximum, drainage-area scaled discharged predicted at this location using the 105 y gage record. Calcluations use $\tau_{*c\_pool} = 0.045$ and the values listed in Table S1.

Table S1. Field-surveyed waterfall plunge pools from Scheingross et al (2016)[†]

River	ID	S	W (m)	H_{drop} (m)	r_{pool} (m)	h_{pool} (m)	D_{50} river (m)	D_{84} river (m)	A (km^2)	UTM East	UTM North	Pool floor	USGS Gage ID	A_{gage} (km^2)	$Q_{s\_river}/Q_{sc\_river} = 1$		$Q_{s\_river}/Q_{sc\_river} = 0.5$		$Q_{s\_river}/Q_{sc\_river} = 0.1$	
															Return period for bedrock ersoion (yr)	**Q_{w_scour} for bedrcok ersoion (m^3/s)**	**Return period for bedrock ersoion (yr)**	**Q_{w_scour} for bedrcok ersoion (m^3/s)**	**Return period for bedrock ersoion (yr)**	**Q_{w_scour} for bedrcok ersoion (m^3/s)**
Colby Canyon	CP1	0.06	5	2.5	2.3	0.9	0.15	0.38	2.62	395326	3792758	sed	11098000	41.40	106*	61**	106*	61.6**	106*	55.1
Colby Canyon	CP2a	0.07	4	2	0.9	0.65	0.15	0.38	1.64	395467	3792855	sed	11098000	41.40	106*	21.1**	106*	21.5**	106*	21.5**
Colby Canyon	CP2b	0.07	4	0.6	1.9	0.4	0.15	0.38	1.64	395467	3792855	sed	11098000	41.40	20	5.8**	20	5.7**	19.8	5.7**
Colby Canyon	CP3	0.06	3	1.2	1.8	0.5	0.15	0.38	1.64	395463	3792879	sed	11098000	41.40	106*	12.1**	106*	12.0**	106*	12.0**
Colby Canyon	CP4b	0.05	3	3.2	1.5	1	0.15	0.38	1.61	395568	3792957	sed	11098000	41.40	106*	53.1**	106*	51.1	106*	26.9
Colby Canyon	CP4c	0.05	3	1.9	2.3	1	0.15	0.38	1.61	395568	3792957	sed	11098000	41.40	106*	24.3**	106*	24.0**	106*	24.0**
Little Santa Anita	LR1	0.08	3.5	8.5	1.0	0.1	0.1	N/A	5.49	403678	3782944	sed	11100500	4.76	N/A[‡]	N/A[‡]	N/A[‡]	N/A[‡]	N/A[‡]	N/A[‡]
Little Santa Anita	LR2	0.08	5	4	2.9	0.5	0.1	N/A	5.49	403681	3782993	?	11100500	4.76	47*	44.8	47*	27.3	31.7	13.0
Little Santa Anita	LR3	0.08	4	3.5	0.7	0.3	0.1	N/A	5.54	403700	3782879	br	11100500	4.76	40	15.6**	41	15.9**	N/A[‡]	N/A[‡]
Little Santa Anita	LR4	0.08	5	8	2.0	1.5	0.1	N/A	5.55	403707	3782848	?	11100500	4.76	13	6.6	N/A[‡]	N/A[‡]	N/A[‡]	N/A[‡]
Little Santa Anita	LR5a	0.08	4	5.5	0.8	1.5	0.1	N/A	5.55	403704	3782825	?	11100500	4.76	N/A[‡]	15.6	N/A[‡]	N/A[‡]	N/A[‡]	N/A[‡]
Little Santa Anita	LR5b	0.08	4	1.25	1.3	1.5	0.1	N/A	5.55	403704	3782825	?	11100500	4.76	45	17.2**	45	17.2**	45.5	17.2**
Little Santa Anita	LD1a	0.08	5	1	0.6	0.24	0.1	N/A	5.59	403707	3782759	br	11100500	4.76	13	6.4**	13	6.4**	12.9	6.4**
Little Santa Anita	LD1b	0.08	5	4	0.7	0.1	0.1	N/A	5.59	403707	3782759	sed	11100500	4.76	34	13.9**	34	13.8**	N/A[‡]	N/A[‡]
Little Santa Anita	LR6	0.08	6	5.2	1.9	2	0.1	N/A	5.6	403719	3782712	?	11100500	4.76	47*	30.2	15	9.6	N/A[‡]	N/A[‡]
Little Santa Anita	LR7a	0.08	6	4.5	1.0	0.3	0.1	N/A	5.6	403675	3782679	sed	11100500	4.76	47*	36.7**	26	11.4	N/A[‡]	N/A[‡]
Little Santa Anita	LR7b	0.08	6	0.75	1.5	1.5	0.1	N/A	5.6	403675	3782679	?	11100500	4.76	28	12.1**	28	12.0**	27.6	12.0**
Little Santa Anita	LDF	0.1	6	1.5	2.1	0.1	0.1	N/A	5.7	403693	3782583	sed	11100500	4.76	47*	34.3**	47*	34.4**	47*	32.5
Little Santa Anita	LR8	0.11	6	4.5	2.0	0.1	0.1	N/A	5.72	403699	3782457	sed	11100500	4.76	47*	54.2	47*	21.3	12.4	5.9
Little Santa Anita	LR9	0.11	5	2.7	2.0	2	0.1	N/A	5.76	403722	3782369	?	11100500	4.76	47*	68.5**	47*	39.9	34.9	14.6
Little Santa Anita	LR10	0.09	3	3	1.5	1	0.1	N/A	5.8	403870	3782433	?	11100500	4.76	47*	37.5	47*	20.9	13.6	7.5
Little Santa Anita	LR11	0.09	2.5	4.7	2.3	4	0.1	N/A	5.82	403910	3782489	?	11100500	4.76	47*	19.8	38	15.8	14.7	9.1
Rubio Canyon	RR1	0.13	4	23	1.9	0.25	0.1	N/A	2.26	397227	3785825	sed	11098000	41.40	N/A[‡]	N/A[‡]	N/A[‡]	N/A[‡]	N/A[‡]	N/A[‡]
Rubio Canyon	RR2	0.13	3	6.5	1.6	0.2	0.1	N/A	2.26	397226	3785809	sed	11098000	41.40	106*	14.6	14	6.4	N/A[‡]	N/A[‡]
Rubio Canyon	RR3	0.13	4	4.6	1.5	0.1	0.1	N/A	2.27	397223	3787590	sed	11098000	41.40	106*	38.3	106*	15.5	7.1	3.5
Rubio Canyon	RR4	0.15	4	6.2	2.3	0.1	0.1	N/A	2.27	397178	3785777	sed	11098000	41.40	106*	26.3	106*	14.7	11.4	5.3
Rubio Canyon	RR5	0.15	3	7.5	2.0	0.1	0.1	N/A	2.27	397172	3785769	sed	11098000	41.40	106*	14.6	36	9.1	6.5	3.0
Rubio Canyon	RR6	0.18	4	8.5	1.4	0.1	0.1	N/A	2.28	397152	3785725	sed	11098000	41.40	38	9.6	6	2.9	N/A[‡]	N/A[‡]

Daisy Canyon	DC1	0.1	2	1.5	0.8	0.3	0.11	0.26	0.75	395633	3792897	sed	11098000	41.40	106*	11.3**	106*	11.4**	106*	11.4**
Daisy Canyon	DC2	0.1	3	2.3	1.3	0.65	0.11	0.26	0.75	395615	3792880	sed	11098000	41.40	106*	32.7**	106*	32.6**	106*	14.3
Daisy Canyon	DC3	0.1	2	1.1	1.0	0.5	0.11	0.26	0.76	395604	3792828	sed	11098000	41.40	106*	7.1**	106*	7.1**	106*	7.1**
Daisy Canyon	DC4	0.1	2	1.5	1.0	0.1	0.11	0.26	0.8	395581	3792807	sed	11098000	41.40	106*	11.3**	106*	11.4**	106*	11.4**
Daisy Canyon	DC5	0.1	2	4	1.0	0.1	0.11	0.26	0.85	395508	3792735	sed	11098000	41.40	106*	25.4	106*	12.7	20.3	3.0
Arroyo Seco	USF	0.035	5	12	7.3	0.5	0.021	0.32	12.08	393659	3791349	sed	11098000	41.40	4	9.7	3	7.4	1.9	4.7
Arroyo Seco (**Reference site**)	MSF	0.035	5	3	4.0	3	0.021	0.32	12.28	393855	3791207	?	11098000	41.40	2	4.3	2	3.2	1.5	2.1
Arroyo Seco	LSF	0.035	5	5	4.4	2	0.021	0.32	12.28	393855	3791207	?	11098000	41.40	2	3.7	2	2.9	1.5	2.0
Arroyo Seco	ASP1	0.014	4	1.21	3.0	0.3	0.021	0.32	12.53	394148	3790733	sed	11098000	41.40	2	4	2	2.9	1.3	1.6
Arroyo Seco	ASP2	0.049	3	1.45	3.0	0.5	0.021	0.32	12.51	394085	3790816	sed	11098000	41.40	2	5.9	2	4.5	1.5	2.4
Arroyo Seco	ASP3	0.052	5	2.18	3.0	0.3	0.021	0.32	12.49	394042	3790846	sed	11098000	41.40	2	4.3	2	3.0	1.3	1.5
Arroyo Seco	ASP4	0.035	5	2.32	3.0	3	0.021	0.32	12.49	394048	3790853	?	11098000	41.40	2	3.1	1	2.2	1.2	1.2
Arroyo Seco	ASP5	0.016	4	1.23	3.0	0.1	0.021	0.32	12.48	394066	3790866	sed	11098000	41.40	2	4.2	2	3.1	1.3	1.7
Fall Creek	FCR1	0.05	3	10.5	1.9	2	0.025	N/A	5.68	392877	3796770	?	11095500	275	3	0.6	2	0.5	N/A‡	N/A‡
Fall Creek	FCR2	0.05	4	12	3.7	0.7	0.025	N/A	5.68	392885	3796758	sed	11095500	275	11	2.9	7	2.2	5.7	1.3
Fall Creek	FCR3	0.05	3	7	3.9	0.55	0.025	N/A	5.68	392890	3796746	sed	11095500	275	14	4	11	3.0	6.2	1.8
Fall Creek	FCR4	0.05	4	23	3.9	0.5	0.025	N/A	5.68	392895	3796728	sed	11095500	275	9	2.8	7	2.1	5.7	1.3
Classic Canyon	CC1	0.12	4	1.5	1.5	0.4	0.05	N/A	1.42	392893	3796323	sed	11095500	275	61*	18.7	61*	10.3	38.7	4.4
Classic Canyon	CCR1	0.12	3	6.5	2.3	0.8	0.05	N/A	1.49	392684	3796459	sed	11095500	275	43	5.2	21	3.3	15.6	1.5
Classic Canyon	CCR2	0.12	3	9	2.3	0.5	0.05	N/A	1.49	392675	3796474	sed	11095500	275	20	3.2	17	2.1	14.3	1.2
Classic Canyon	CCR2a	0.12	3	2	1.4	1.3	0.05	N/A	1.49	392675	3796474	br	11095500	275	61*	11.3	44	5.3	18.3	2.5
Classic Canyon	CCR2b	0.12	3	2	1.6	0.3	0.05	N/A	1.49	392675	3796474	sed	11095500	275	61*	11.3	53	6.5	20.4	3.3
Fox Creek	FXR1	0.05	2	3	2.3	1	0.03	0.05	22.75	391431	3797425	br	11095500	275	2	1.9	2	1.3	1.4	0.5
Fox Creek	FXR2	0.05	5	13	3.5	0.75	0.03	0.05	22.75	391467	3797391	sed	11095500	275	3	2.6	2	2.0	2.0	1.2
Fox Creek	FXR3	0.05	3	3.5	3.5	1	0.03	0.05	22.75	391482	3797388	sed	11095500	275	6	6.1	5	4.4	2.7	2.5
Fox Creek	FXR4	0.05	3.6	7.5	3.4	0.85	0.03	0.05	22.75	391495	3797399	sed	11095500	275	3	2.9	3	2.2	2.2	1.4
Fox Creek	FXR5	0.05	4	3.5	2.8	0.7	0.03	0.05	22.75	391501	3797420	sed	11095500	275	4	3.6	3	2.5	2.2	1.3
Fox Creek	FXR6	0.05	7	27	2.0	0.5	0.03	0.05	22.75	391565	3797461	sed	11095500	275	N/A‡	N/A‡	N/A‡	N/A‡	N/A‡	N/A‡
Fox Creek	FXR7	0.05	4	6	3.0	2	0.03	0.05	22.75	391582	3797472	?	11095500	275	3	2.3	2	1.8	2.1	1.2
Fox Creek	FXR8	0.05	4	3.5	3.5	0.7	0.03	0.05	22.75	391611	3797487	sed	11095500	275	6	6	5	4.3	2.7	2.4
Fox Creek	FXR9	0.05	5	16	3.5	0.5	0.03	0.05	24.6	391524	3796514	sed	11095500	275	3	2.5	2	1.9	2.0	1.1
Millard Canyon	M1	0.075	5	17	2.9	0.3	0.05	N/A	5.1	394833	3787038	sed	11098000	41.40	2	2.4	2	1.7	N/A‡	N/A‡
Wolfskill Canyon	W1	0.1	6	9	5.0	1.2	0.17	0.13	5.2	430738	3781897	sed	N/A⁑	5.40	8	113.5	6	80.6	3.1	36.4

Dry Meadow Ck	STC1	0.05	12	2.66	6.2	3.9	0.1	N/A	93.5	366139	3984275	?	11186000	2191	111*	147.1	111*	117.6	109.0	71.9
Dry Meadow Ck	STC2	0.05	12	3.74	4.8	2	0.1	N/A	93.5	366143	3984266	?	11186000	2191	111*	90.9	91	66.5	26.9	32.1
Dry Meadow Ck	STC3	0.05	12	5.34	9.2	5	0.1	N/A	93.5	366146	3984250	sed	11186000	2191	111*	170.9	111*	125.8	89.9	66.2
Dry Meadow Ck	STC4	0.05	12	3.89	5.9	4.62	0.1	N/A	93.5	366155	3984237	sed	11186000	2191	111*	113.9	111*	84.1	44.8	42.6
Dry Meadow Ck	STC5	0.05	12	1.24	4.9	2.21	0.1	N/A	93.5	366159	3984225	br	11186000	2191	51	50.7**	51	50.7**	51.3	50.7**
Dry Meadow Ck	STC6	0.05	12	2.85	7.4	2.53	0.1	N/A	93.5	366166	3984219	?	11186000	2191	111*	178.3	111*	141.7	111*	85.8
Dry Meadow Ck	STC7	0.05	12	2.36	4.5	2.55	0.1	N/A	93.5	366175	3984206	sed	11186000	2191	111*	133.7**	111*	101.4	65.1	58.8
Dry Meadow Ck	STC8	0.05	12	11	4.4	1.35	0.1	N/A	93.5	366191	3984207	?	11186000	2191	N/A‡	N/A‡	N/A‡	N/A‡	N/A‡	N/A‡
Dry Meadow Ck	STC9	0.05	12	13.99	6.4	3.57	0.1	N/A	93.5	366246	3984191	?	11186000	2191	19	23.2	12	14.4	N/A‡	N/A‡
Kapaa Stream	HFU	0.007	12	6	4.0	3	0.15	0.62	16.8	464537	2444738	?	16060000	61.50	N/A‡	N/A‡	N/A‡	N/A‡	N/A‡	N/A‡
SF Wailua River	WF	0.006	12	49	40.0	10	0.1	N/A	62	460951	2436662	?	16060000	61.50	2	358.1	2	300.6	1.3	213.8
Huleia Stream	KP	0.003	10	5.6	22.3	7.5	0.2	N/A	47	456876	2427414	?	16055000	46.83	15	414.2**	14	404.8**	11.0	367.7
Kaulaula Valley	KA	0.13	6	39	3.7	0.2	0.3	N/A	3.2	425986	2442220	?	16130000	9.81	N/A‡	N/A‡	N/A‡	N/A‡	N/A‡	N/A‡
Hanakapiai Stream	HF	0.4	10	120	22.0	4.7	0.3	N/A	4.5	438743	2453474	?	16115000	7.10	21*	40100**	21*	1630.1	21*	468.5

† S - reach-averaged channel slope, W - reach-averaged channel width upstream of the waterfall, H_{drop} - waterfall drop height, r_{pool} - plunge-pool radius, D_{50} and D_{84} - estimate of median and 84 percentile grain size for the river reach, respectively. Grain size data comes from a mix of visual estimates and pebble counts, in cases where pebble counts were performed, we report both D_{50} and D_{84}, for visual estimates, we report D50 only. h_{pool} - plunge pool depth (note: the "pool floor" column indicates if depth was to sediment, "sed", to bedrock, "br", or unknown, "?"), A and A_{gage} - drainage area at waterfall and discharge gaging station, respectively, Q_{w_scour} - Threshold discharge above which pools will scour to their bedrock floors.

* Recurrance interval of the threshold discharge for scour to bedrock was greater than the length of record at the gaging station and was set to the length of the record.

** Minimum estimate of the threshold discharge to scour to bedrock as the waterfall becomes submerged before the threshold discharge is reached.

⁑ 21-year discharge record for Wolfskill Falls from 1939-1959 provided by the US Forest Service.

‡ No value of Q_{w_scour} calculated as pool sediment transport capacity was greater than river sediment transport capacity for all discharges, likely indicating a disequilibrium bedrock geometry of the waterfall plunge pool.

Table S2: Individual clast measurements for grain size distributions shown in Figure 1*

Particle diameter (cm)							
Arroyo Seco					Wolfskill Falls		
Channel	Pool 1	Bar 1	Pool 2	Bar 2	Channel	Pool	Bar
48	1	8	0.1	40	20	2	10
6	1	9	0.1	22	4	0.8	8
50	0.5	48	0.3	13	24	1.8	28
17	2	85	3.2	35	1	1.5	20
46	1	3	1.5	6	2	1.5	3
0.6	1	4	4.5	0.1	3	4.5	4
222	2	1	7.5	75	20	4	25
1.7	4	20	1.2	8	2	3	21
0.3	2	45	11	1	3	0.1	15
9.3	4	44	4	13	10	2	16
1.2	2	66	5	45	3	1.5	18
2.1	6	45	10.5	0.1	0.5	1	16
1.6	2	85	0.1	0.1	2	0.1	10
0.6	1	8	2	0.1	10	0.1	20
0.6	2	35	10	90	1	0.8	25
0.8	0.6	70	21	0.1	2	20	16
2.4	2	30	2.5	0.1	1	0.9	12
0.7	0.3	6	4	40	1	1.2	12
0.9	3.5	23	0.1	2	20	0.4	26
4.1	0.8	15	2	2	23	1.1	23
4	4	30	0.8	2	2	0.5	17
30	2.5	4	13	1	3	70	26
120	1.2	3	3.5	0.1	2	1.5	22
0.6	7.5	15	0.5	2	2	0.5	14
47	2	30	5.5	4	5	0.1	19
1.6	1.2	0.1	2.5	110	4	0.1	10
1.1	1.8	20	0.1	25	2	0.1	12
1	0.5	12	1.1	17	1	0.1	6
4.2	0.3	11	5.5	35		0.1	10
42	0.5	55	3.5	45		0.1	27
3.1	0.8	0.5	2.1	0.1		8	11
1.4	0.3	3	0.1	0.1		0.1	28
1.6	3	6	0.1	45			32
0.9	2	45	2	0.1			27
2.1	0.1	28	1.5	0.1			18
43	0.6	80	0.1	0.1			7
4.9	0.3	0.5	5.5	0.1			25
8.8	4.5	0.1	5	42			10
7.6	1.2	4	6	3			13
2.1	2.5	0.5	1	70			7
2.2	6	2	0.5	42			7
3.2	2.5	50	4	10			22
2.6	1.5	30	0.5	0.1			30

0.6	2	35	0.2	65	17
0.4	2	60	1	0.1	8
1.2	0.3	2	2	3	15
0.3	0.5	4	0.1	70	30
2.7	1.2	38	0.2	8	15
0.8	1.5	22.1	2	30	11
1.1	0.2	41	0.1	90	12
2.1	0.1	2.5	5	5	17
4.5	0.1	50	1.5	55	10
5.1	2		8	5	16
4.1	0.5		5	0.1	19
3.2	1.2		1.5	50	18
0.5	0.2		4.5	0.1	15
0.9	0.2		1.5	0.1	24
0.5	1.5		7	50	18
0.5	2		2.5	0.2	13
4	0.1		2.5		12
18	1.2		7		11
52	0.1		1.5		6
0.2	2		0.1		
40	1.6		0.1		
80	1.2		0.1		
80	0.7		0.3		
4.2	4		2		
1.5	2.5		2		
2.2	1.5		5		
0.4	1.8		3.5		
1.6	2.5		4		
	1.3		2.5		
	1		0.5		
	2		1.5		
	1.5		8		
	0.8		2		
	1.2		1.5		
	1.5		3.5		
	0.1		1.5		
	0.1		5		
	1.2		0.7		
	0.5		1.1		
	0.2		2.6		
	2.2		1.2		
	0.3		8		
	0.5		5		
	1.5		1		
	0.5		2.5		
	0.1		1.5		
	0.1		0.1		

3.3	0.2	
1.5	0.4	
0.8	1.5	
1.5	4.2	
1.2	0.1	
1	0.1	
	0.1	
	0.1	

* All grain size measurements on Arroyo Seco and Wolfskill Falls made on 17 March 2010 and 12 March 2010, respectively . Grain size counts were conducted either by via a heel-toe random walk or stretching a measuring tape and measuring grains every 0.5 m. Arroyo Seco Pool/Bar 1 and Pool/Bar 2 are separated by less than 100 m and the channel grain size measurements was taken in the fluvial reach between the two waterfall plunge pools. At Wolfskill Falls the channel measurements were taken in a short (~ 3 m) section between the downstream bar and a subsequent dowstream waterfall, limiting the total number of grain size measurements.